

(TITLE UNCLASSIFIED)

**PRESSURE DISTRIBUTION AND FORCE COEFFICIENTS
MEASURED ON THE APOLLO COMMAND-MODULE
RE-ENTRY CONFIGURATION AT MACH NUMBER 19**

By

Eugene C. Knox
von Kármán Gas Dynamics Facility
ARO, Inc.

TECHNICAL DOCUMENTARY REPORT NO. AEDC-TDR-62-193

October 1962

AFSC Program Area 921E, Project 9071

(Prepared under Contract No. AF 40(600)-1000 by ARO, Inc.,
contract operator of AEDC, Arnold Air Force Station, Tenn.)

**ARNOLD ENGINEERING DEVELOPMENT CENTER
AIR FORCE SYSTEMS COMMAND
UNITED STATES AIR FORCE**

(NASA-CR-118611) PRESSURE DISTRIBUTION AND
FORCE COEFFICIENTS MEASURED ON THE APOLLO
COMMAND-MODULE RE-ENTRY CONFIGURATION AT
MACH NUMBER 19 (ARO, Inc.) 26 p

N79-76123

Unclas
11640

00/02

AVAILABLE TO GOVERNMENT AGENCIES
AND CONTRACTORS ONLY

AVAILABLE TO GOVERNMENT AGENCIES AND CONTRACTORS ONLY

DOWNGRADED AT 3 YEAR INTERVALS;
DECLASSIFIED AFTER 12 YEARS.
DOD FORM 9200-10

~~CONFIDENTIAL~~

(Title Unclassified)
PRESSURE DISTRIBUTION AND FORCE COEFFICIENTS
MEASURED ON THE APOLLO COMMAND-MODULE
RE-ENTRY CONFIGURATION AT MACH NUMBER 19

By
Eugene C. Knox
von Kármán Gas Dynamics Facility
ARO, Inc.
a subsidiary of Sverdrup and Parcel, Inc.

CLASSIFICATION CHANGE
To UNCLASSIFIED
By authority of GDS-P-11612
Changed by L. Shirley Date 12/7/72
Classified Document Master Control Station, NASA
Scientific and Technical Information Facility

October 1962
ARO Project No. 304244

~~CONFIDENTIAL~~

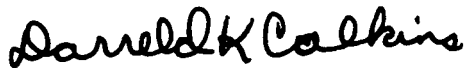
(This abstract is UNCLASSIFIED.)

ABSTRACT

Pressure distribution and force tests were made on an Apollo command-module re-entry configuration in the 50-in. Hypervelocity Tunnel (HS-2) at Mach number 19 and a Reynolds number of about 85,000 based on model maximum diameter. Angle of attack ranged from 0 to 60 deg.

PUBLICATION REVIEW

This report has been reviewed and publication is approved.



Darreld K. Calkins
Major, USAF
AF Representative, VKF
DCS/Test



Jean A. Jack
Colonel, USAF
DCS/Test

CONTENTS

	<u>Page</u>
ABSTRACT	ii
NOMENCLATURE	v
1.0 INTRODUCTION	1
2.0 APPARATUS	
2.1 Wind Tunnel	1
2.2 Models	1
2.3 Instrumentation	2
2.4 Precision	2
3.0 RESULTS AND DISCUSSION	
3.1 PS-4 Pressure Model	3
3.2 FS-4 Force Model	4
4.0 CONCLUDING REMARKS	4
REFERENCES	5

TABLES

1. Arc-Chamber and Test Section Conditions	6
2. Pressure Ratios (p/p_0') for PS-4 Model	7

ILLUSTRATIONS

Figure

1. The 50-in. Hypervelocity Tunnel (Hotshot 2)	8
2. Descriptive Model Drawings	
a. PS-4 Model	9
b. FS-4 Model	10
3. Model Photographs	
a. PS-4 Model Showing Inside of Model	11
b. PS-4 Installed in Tunnel.	12
c. FS-4 Showing Balance Mounting	13
d. FS-4 Installed in Tunnel.	14
4. Sketch of PS-4 Showing Pressure Orifice Locations . .	15
5. Measured Pressure Distribution on PS-4	
a. $\alpha = 0$ deg	16
b. $\alpha = 20$ deg	16
c. $\alpha = 40$ deg	16
d. $\alpha = 60$ deg	16

<u>Figure</u>	<u>Page</u>
6. Sketch of Model Showing Positive Directions of Model Coefficients.	17
7. Data Plots of C_L , C_D , and $C_{m_{cg}}$	18
8. Typical Schlieren Photograph of PS-4 Model	19

NOMENCLATURE

C_{AM}	Axial-force coefficient in model axis
C_D	Model drag coefficient
C_L	Model lift coefficient
$C_{m_{cg}}$	Pitching-moment coefficient about reference center of gravity
C_{NM}	Normal-force coefficient in model axis
d	Model maximum diameter, 6.160 in.
d^*	Tunnel throat diameter, in.
M_∞	Free-stream Mach number
p	Local static pressure on model, psia
p_∞	Free-stream static pressure, psia
p_0	Reservoir pressure, psia
p_0'	Total pressure behind normal shock in test section, psia
q_∞	Free-stream dynamic pressure, psia
R	Model maximum radius, 3.08 in.
Re_∞	Free-stream Reynolds number based on model maximum diameter
S_π	Reference area, 29.8 in. ²
s/R	Ratio of surface distance measured from heat-shield center to model maximum radius
T_∞	Free-stream temperature, °K
T_0	Reservoir temperature, °K
V_∞	Free-stream velocity, fps
α	Model angle of attack referenced to center of heat shield, deg
λ	Angle of orifice meridional plane reference to vertical, deg
η	Turning angle between velocity vector and local body tangent, deg
ρ_∞	Free-stream density, atm
ρ_0	Reservoir density, atm (reference density = 0.0780641 lb/ft ³)

1.0 INTRODUCTION

At the request of the Manned Spacecraft Center, NASA, Houston, Texas, through North American Aviation, Inc., Space and Information Systems Division, Downey, California, pressure distribution and force tests were conducted with the PS-4 and FS-4 Apollo command-module re-entry configurations in the 50-in. Hypervelocity Tunnel (Hotshot 2) of the von Kármán Gas Dynamics Facility (VKF), Arnold Engineering Development Center (AEDC), Air Force Systems Command (AFSC), USAF, during the period from June 18 to July 11, 1962. The test Mach number was approximately 19 and the Reynolds number was about 0.085×10^6 based on model maximum diameter (6.16 in.). The model angle of attack ranged from 0 to 60 deg.

The purpose of these tests was to obtain experimental pressure, force, and moment data on the Apollo re-entry configuration at extreme hypersonic Mach numbers. These tests are part of a general test program to document experimentally the aerodynamic characteristics of the Apollo vehicle over a wide range of test conditions compatible with the expected flight regime.

2.0 APPARATUS

2.1 WIND TUNNEL

The 50-in. Hypervelocity Tunnel (Hotshot 2), Fig. 1, is an arc-driven, blowdown wind tunnel with a 50-in. -diam test section. Nitrogen, initially confined in the arc chamber, is heated and pressurized to approximately 3500°K and 10,000 psia by generating an electric arc in the chamber. Upon rupture of a mylar diaphragm, the heated gas expands through a conical nozzle to the test section where Mach numbers of approximately 19 are obtained. Additional description of this tunnel is included in Ref. 1. Copper arc-chamber liners and semicon-tungsten throats, 0.281 inch in diameter, were used for these tests.

2.2 MODELS

The PS-4 (pressure) and FS-4 (force) models were supplied by the Space and Information Systems Division, North American Aviation, Inc., Downey, California. Drawings of these models are presented in Figs. 2a and b, and Figs. 3a through d are pictures of the models.

Manuscript released by author September 1962.

2.3 INSTRUMENTATION

The PS-4 model was instrumented to measure surface pressures with variable-reluctance-type transducers mounted inside the model within 0.5 in. of their corresponding orifices at the model surface to give a rapid time response.

The test section pitot pressure was measured at points 6 in. above and below the tunnel centerline. The arc-chamber pressure was measured at two points within the chamber with strain-gage-type, high pressure transducers. Also, schlieren photographs and Fastax movies were taken during each run.

The FS-4 model was instrumented with a three-component, strain-gage-type balance aligned at 30 deg to the model axis of symmetry in an effort to minimize sting interference at high angles of attack. The three components of force which were measured are an aft and forward normal force and an axial force. The two normal-force gages were connected with a compensation network in an effort to minimize sting-oscillation acceleration effects. The compensation system was effective, and the data obtained by this means were used in all but two of the force runs (0 and 20 deg).

A complete discussion of the instrumentation used in the hotshot tunnels and a discussion of the compensation technique are given in Refs. 2 and 3.

2.4 PRECISION

The response of the variable-reluctance pressure transducers is linear within ± 2 percent. This variation results in an overall repeatability in p/p_0 of ± 5 percent.

The repeatability of the force measurements during static calibration was within ± 1 percent of the rated load, which is 20 lb on all gages. In conjunction with other random errors, the increment of uncertainty in the force measurement is about 0.05 in coefficient form. In all cases, the measured timewise variation of the coefficients was within ± 5 percent.

3.0 RESULTS AND DISCUSSION

The arc-chamber and test section conditions are tabulated in Table 1 for each run. The values presented are averaged over the time interval

during which quasi-steady flow was established in the test section. Table 2 is a tabulation of p/p'_0 for each orifice on PS-4 for each of the test angles of attack. A sketch of the PS-4 model denoting the orifice locations is presented in Fig. 4. The places where a dashed line is shown in Table 2 denote that the local pressure was too low (less than 0.03 psia) for the transducer to measure reliably, with the exception of orifice 67. The transducer for that orifice failed after Run 1239.

3.1 PS-4 PRESSURE MODEL

Before the discussion of the pressure results is made, a few words regarding observed gage reliability and run-to-run repeatability are warranted. The gage reliability can be determined by comparison of the results in Table 2 for either Run 1236 or 1245. The measurements at equal s/R values but different meridians show a ± 5 percent variation. Likewise, a comparison of Runs 1236 and 1245 or 1239 and 1240 exhibit a run-to-run repeatability of ± 5 percent.

Typical pressure distributions for selected angles of attack are presented in Fig. 5. Also shown in Fig. 5 is a theoretical distribution computed from modified Newtonian theory, which is

$$p/p'_0 \approx \sin^2 \eta$$

neglecting p_∞ which introduces only a 5 percent error whenever the local pressure is as low as 0.03 psia. The scale along the radial lines is one in. equals a p/p'_0 of unity, and the symbol size reflects a ± 0.05 variation in p/p'_0 ; hence, for values near unity the symbol covers the range of uncertainty in the experimental results.

As can be seen in Fig. 5, within the experimental uncertainty there is good agreement with modified Newtonian theory, except in the shoulder regions. The lack of agreement in the shoulder region would be expected inasmuch as the sonic point near the shoulder is established ahead of that predicted by Newtonian theory. This phenomenon was observed in Ref. 4, which is a general parametric study of blunt bodies, as well as on the Mercury configuration, as presented in Ref. 5.

At high angles of attack on the windward side of the model at the shoulder, there is a strong interaction of the bow shock with the shoulder, resulting in a stagnation point shift toward the center of the heat shield, away from that predicted by Newtonian theory. This shift causes the pressure on the windward side of the heat shield to be higher than theory. The interaction can be seen in a typical schlieren presented in Fig. 8.

3.2 FS-4 FORCE MODEL

In the previous section it was shown that the experimental pressure fell significantly below the theoretical results in the shoulder region for low angles of attack. In fact, this effect is large enough to cause a 20 percent discrepancy between the measured drag coefficient and that computed by the theory. For this reason, then, the Newtonian force predictions are not included in Fig. 7, which is a summary of the force results. Instead, the present data are compared with the results at Mach 9 presented in an unpublished North American Aviation report on the FS-1 configuration. These results are shown as a faired solid curve in Fig. 7. Regarding the comparison of the present data with the Mach 9 results, the axis systems for the present results were re-oriented such that the heat shield being windward corresponds to $\alpha = 0$ rather than 180 deg which is the system used for the Mach 9 data. Figure 6 shows the positive directions of the model coefficients and the position of the cg considered for the present tests.

Examination of Fig. 7 shows that the present data agree very well with the Mach 9 data, indicating an insignificant Mach number effect between Mach 9 and 19. The present data indicate that the FS-4 configuration trims at an angle of attack of about 35 deg with trim lift and drag coefficients of -0.49 and 0.97, respectively. These values yield an $(L/D)_{\text{trim}} = -0.505$ and a trim static margin of 0.487d.

4.0 CONCLUDING REMARKS

The results of the present investigation show that the pressure distribution on the Apollo shape can be adequately predicted by Newtonian theory, that to a first-order approximation the Newtonian theory can be used to predict the forces on the Apollo configuration, and that there appears to be no significant Mach number effect between Mach 9 and 19 on the pressure and force results for the Apollo shape.

REFERENCES

1. Test Facilities Handbook, (Fourth Edition). "von Kármán Gas Dynamics Facility, Vol. 4." Arnold Engineering Development Center, July 1962.
2. Earheart, W. T., Jr., and Bynum, D. S. "Hypervelocity Arc-Tunnel Instrumentation." AEDC-TN-60-227, December 1960.

3. Edenfield, E. E. and Ledford R. L. "Compensation of Dynamic Sting Effects in Hotshot Force Measurements." AEDC-TDR-62-122, June 1962.
4. Boison, J. C. and Curtiss, H. A. "An Experimental Investigation of Blunt Body Stagnation Point Velocity Gradient." Journal of the American Rocket Society, Vol. 29, No. 2, February 1959, pp. 130-135.
5. Reller, John O., Jr., and Seegmiller, H. Lee. "Pressure and Heat-Transfer Measurements on a Mercury Capsule Model." NASA-TM-X-647, May 1962. CONFIDENTIAL

TABLE 1
ARC-CHAMBER AND TEST SECTION CONDITIONS

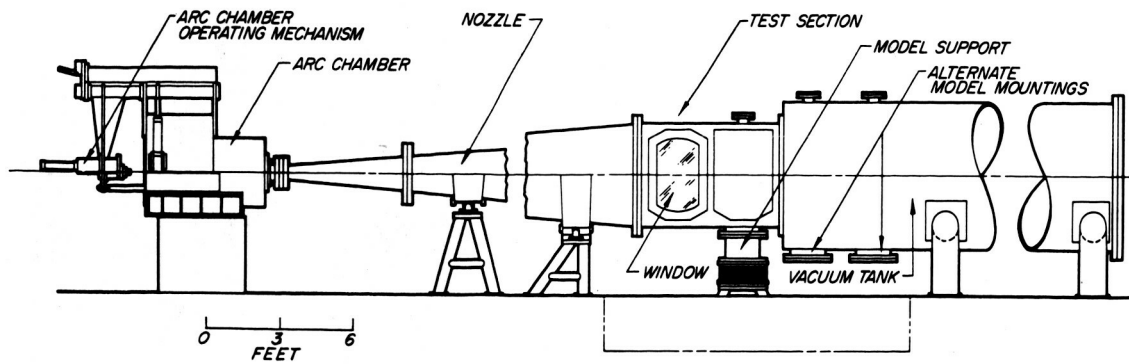
Nominal Shots: $P_{0max} = 10,000$ psia, $\rho_{0max} = 50$ atm, $T_{0max} = 3500^\circ K$, with N_2 , $d^* = 0.281$ in.

Run No.	Model Config.	α , deg	P_0 , psia	ρ_0 , atm	T_0 , $^\circ K$	M_∞	Re_∞ (Model)	V_∞ , fps	$P_\infty \times 10^3$, psia	$\rho_\infty \times 10^3$, atm	T_∞ , $^\circ K$	q_∞ , psia	P'_0 , psia
1236	PS-4	0	6,800	41.00	3,000	18.94	88,418	8,599	1.38	0.54	47.00	0.344	0.643
1237	"	10	7,094	41.17	3,032	18.99	84,754	8,751	1.37	0.53	49.48	0.344	0.684
1238	"	20	6,599	40.95	2,837	19.19	88,702	8,469	1.25	0.53	44.29	0.320	0.606
1239	"	30	7,075	40.57	3,071	18.80	83,997	8,914	1.48	0.55	50.26	0.365	0.680
1240	"	30	6,562	38.66	2,994	18.91	81,311	8,737	1.33	0.53	48.71	0.331	0.637
1241	"	40	6,550	38.96	2,965	18.87	83,167	8,705	1.35	0.54	48.36	0.336	0.625
1242	"	50	6,030	39.18	2,714	19.28	88,402	8,356	1.16	0.51	41.82	0.302	0.561
1243	"	60	6,669	40.75	2,882	19.26	85,488	8,612	1.23	0.51	44.70	0.319	0.594
1244	"	33	6,835	38.71	3,115	18.75	78,942	8,985	1.42	0.53	51.70	0.348	0.673
1245*	"	0	4,656	40.53	2,023	19.89	123,652	7,096	0.88	0.57	28.46	0.242	0.450
1256	FS-4	0	7,134	40.16	3,129	18.70	82,510	8,830	1.44	0.54	49.64	0.353	0.658
1257	"	20	5,814	37.22	2,772	18.96	85,968	8,379	1.22	0.53	44.35	0.306	0.569
1259	"	30	5,820	37.60	2,734	18.48	94,648	8,475	1.54	0.60	45.52	0.367	0.683
1260	"	40	6,567	37.34	3,106	18.80	76,200	9,054	1.41	0.48	50.18	0.348	0.649
1261	"	50	6,122	37.32	2,897	18.87	82,246	8,636	1.30	0.51	46.61	0.324	0.602
1263	"	60	7,808	37.71	3,656	18.50	65,178	9,806	1.64	0.48	62.77	0.392	0.731
1264	"	10	6,601	38.94	2,989	18.66	85,173	8,773	1.47	0.55	49.42	0.359	0.687

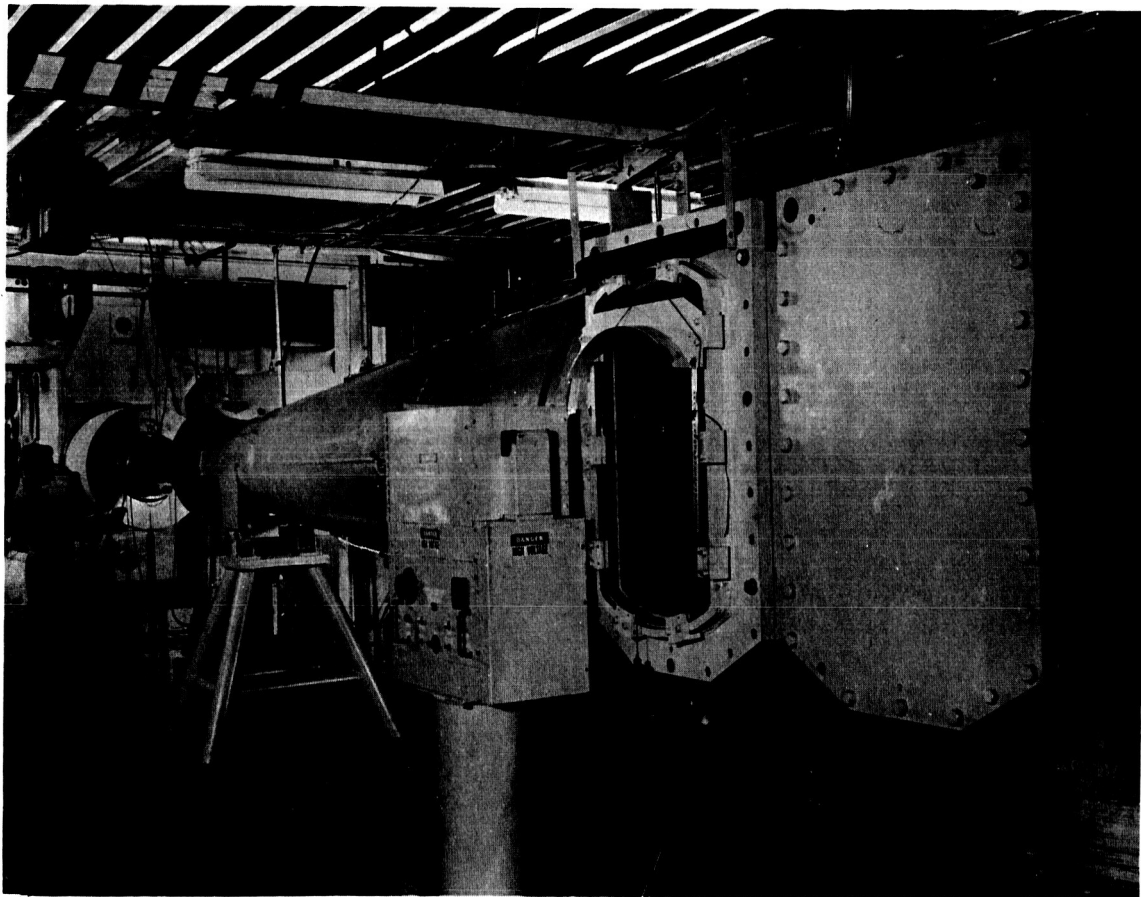
* Cold shot: inviscid pressure distribution unaffected; however, free-stream conditions not comparable.

TABLE 2
PRESSURE RATIOS (p/p_o) PS-4 MODEL

Orifice Number	Orifice Meridian	Orifice Location, s/R	$\alpha = 0^\circ$	$\alpha = 10^\circ$	$\alpha = 20^\circ$	$\alpha = 30^\circ$	$\alpha = 30^\circ$	$\alpha = 40^\circ$	$\alpha = 50^\circ$	$\alpha = 60^\circ$	$\alpha = 33^\circ$	$\alpha = 0^\circ$
Run 1236												
2	$\lambda = 0^\circ$	2.566	-	-	-	-	-	-	0.056	0.179	-	1245
3		2.179	-	-	-	-	-	-	0.073	0.202	-	-
4		1.791	-	-	-	-	-	-	0.089	0.224	-	-
5		1.404	-	-	-	-	-	0.051	0.129	0.239	0.048	-
6		1.084	-	0.050	0.117	0.220	0.223	0.076	0.129	0.239	0.048	-
7		0.984	0.476	0.591	0.728	0.870	0.846	0.382	0.597	0.845	0.256	-
8		0.897	0.767	0.880	0.948	0.978	0.974	0.985	1.000	0.929	0.873	0.509
9		0.712	0.868	1.020	1.002	0.981	0.981	1.000	0.919	0.791	0.985	0.786
10		0.530	0.888	0.993	0.959	0.910	0.910	0.953	0.824	0.651	1.000	0.941
11		0.352	0.939	0.999	0.962	0.839	0.889	0.771	0.623	0.446	0.897	0.986
12		0.175	0.958	1.005	0.915	0.791	0.786	0.678	0.511	0.345	0.772	1.012
13		0	0.993	0.833	0.825	0.718	0.679	0.568	0.409	0.250	0.669	1.000
86		-1.084	-	-	-	-	-	-	-	-	-	-
87		-0.984	0.447	0.384	0.306	0.200	0.194	0.136	0.072	-	0.176	0.435
88		-0.897	0.727	0.641	0.484	0.331	0.328	0.220	0.126	0.066	0.301	0.736
89		-0.712	0.913	0.737	0.575	0.406	0.430	0.262	0.163	0.082	0.353	0.916
90		-0.530	0.926	0.811	0.650	0.477	0.471	0.341	0.219	0.126	0.434	0.914
91		-0.352	0.939	0.868	0.716	0.545	0.536	0.395	0.258	0.161	0.499	0.962
92		-0.175	0.993	0.924	0.799	0.631	0.633	0.501	0.358	0.219	0.606	1.013
23	$\lambda = 45^\circ$	2.179	-	-	-	-	-	-	-	0.088	-	-
25		1.404	-	-	-	-	-	-	0.063	0.111	-	-
26		1.084	-	0.060	0.093	0.135	0.138	0.204	0.294	0.392	0.157	-
27		0.984	0.497	0.578	0.629	0.733	0.662	0.720	0.707	0.668	0.690	0.501
29		0.712	0.866	0.945	0.909	0.860	0.881	0.795	0.666	0.511	0.829	0.884
31		0.352	1.008	1.003	0.915	0.806	0.825	0.701	0.545	0.373	0.789	0.991
66		-1.084	-	-	-	-	-	-	-	-	-	-
67		-0.984	0.493	0.432	0.356	0.252	-	-	-	-	-	-
69		-0.712	0.873	0.779	0.620	0.458	0.447	0.323	0.134	0.120	0.420	0.886
71		-0.352	0.945	0.891	0.748	0.590	0.582	0.450	0.309	0.188	0.532	0.984
45	$\lambda = 90^\circ$	1.404	-	-	-	-	-	-	-	-	-	-
46		1.084	-	-	-	-	-	-	-	-	-	-
47		0.984	0.517	0.488	0.512	0.373	0.373	0.301	0.234	0.159	0.353	0.519
49		0.712	0.875	0.863	0.771	0.639	0.665	0.517	0.384	0.245	0.616	0.901
51		0.352	0.995	1.002	0.877	0.740	0.708	0.565	0.411	0.266	0.648	0.980
129		-0.712	0.915	0.874	0.791	0.647	0.654	0.523	0.379	0.241	0.580	0.934

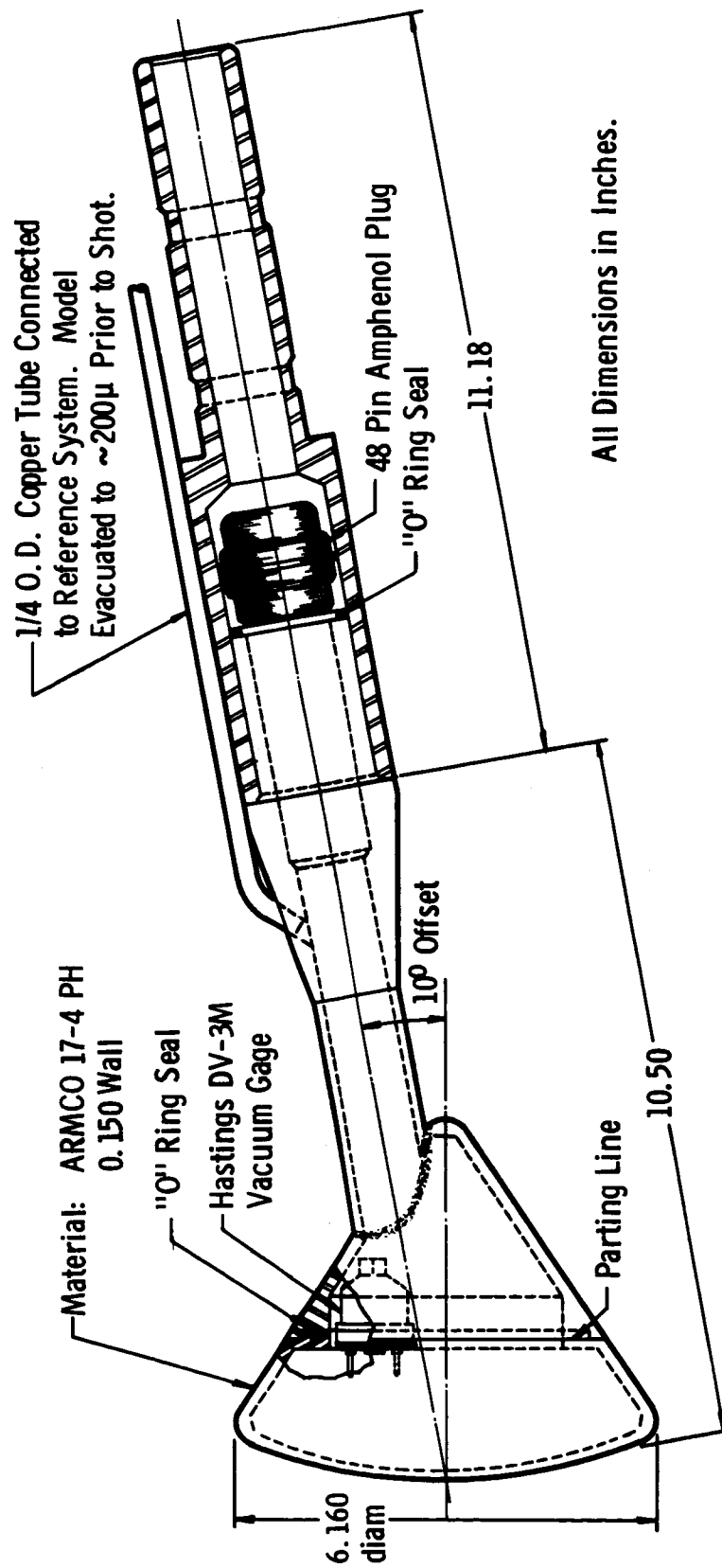


Assembly



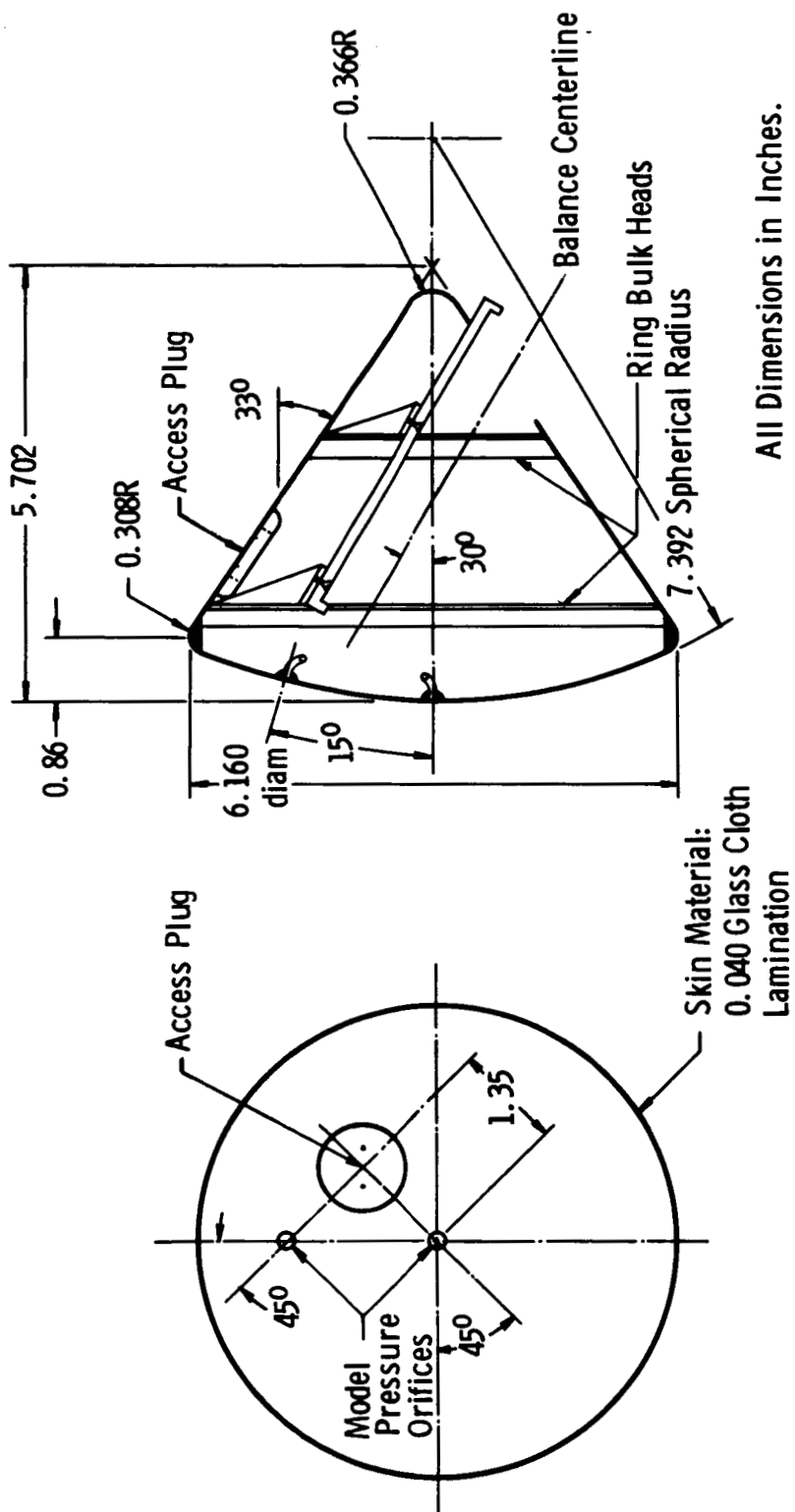
Arc Chamber, Nozzle, and Test Section

Fig. 1 The 50-in. Hypervelocity Tunnel (Hotshot 2)



a. PS-4 Model

Fig. 2 Descriptive Model Drawings



b. FS-4 Model

Fig. 2 Concluded



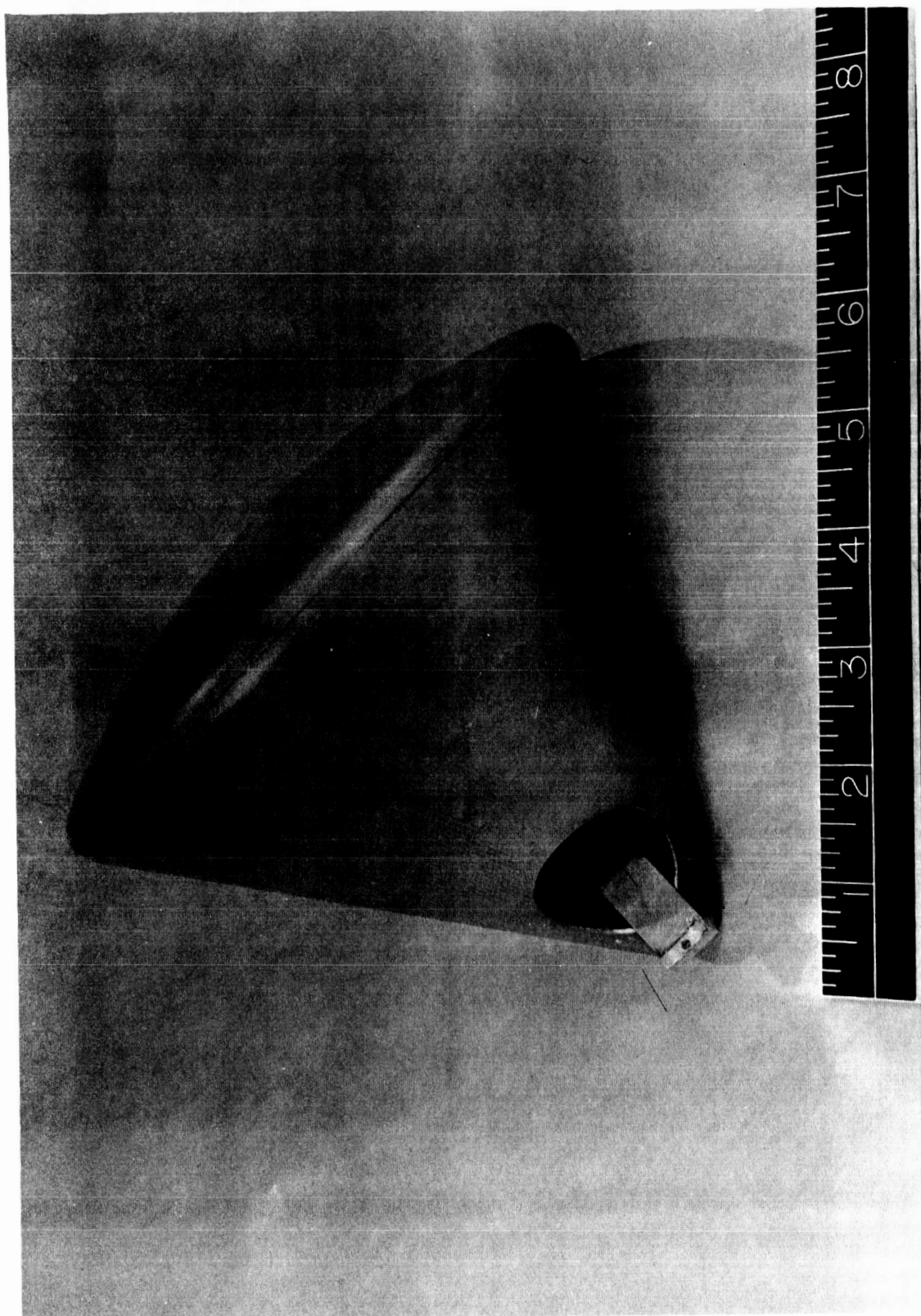
a. PS-4 Model Showing Inside of Model

Fig. 3 Model Photographs



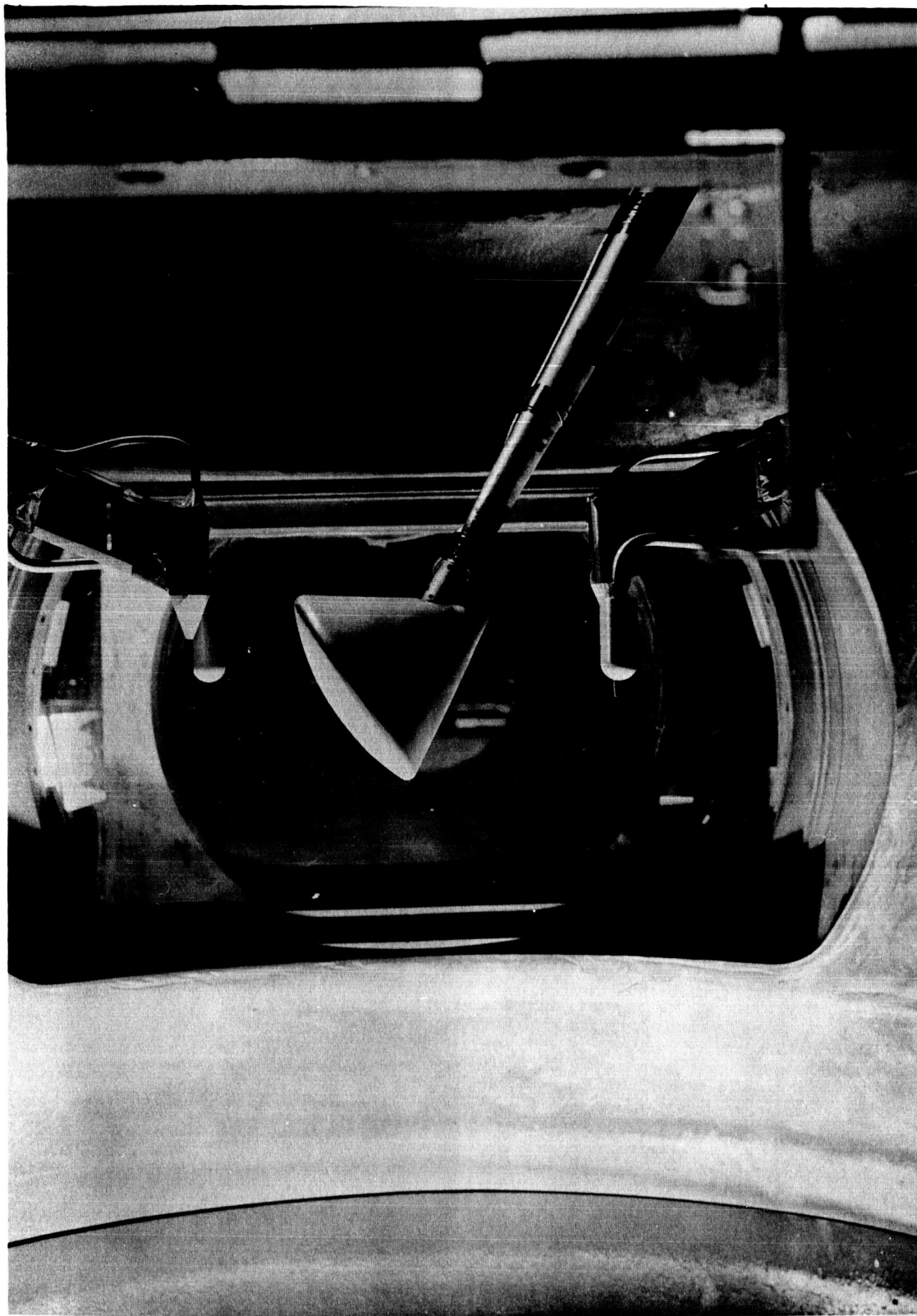
b. PS-4 Installed in Tunnel

Fig. 3 Continued



c. FS-4 Showing Balance Mounting

Fig. 3 Continued



d. FS-4 Installed in Tunnel

Fig. 3 Concluded

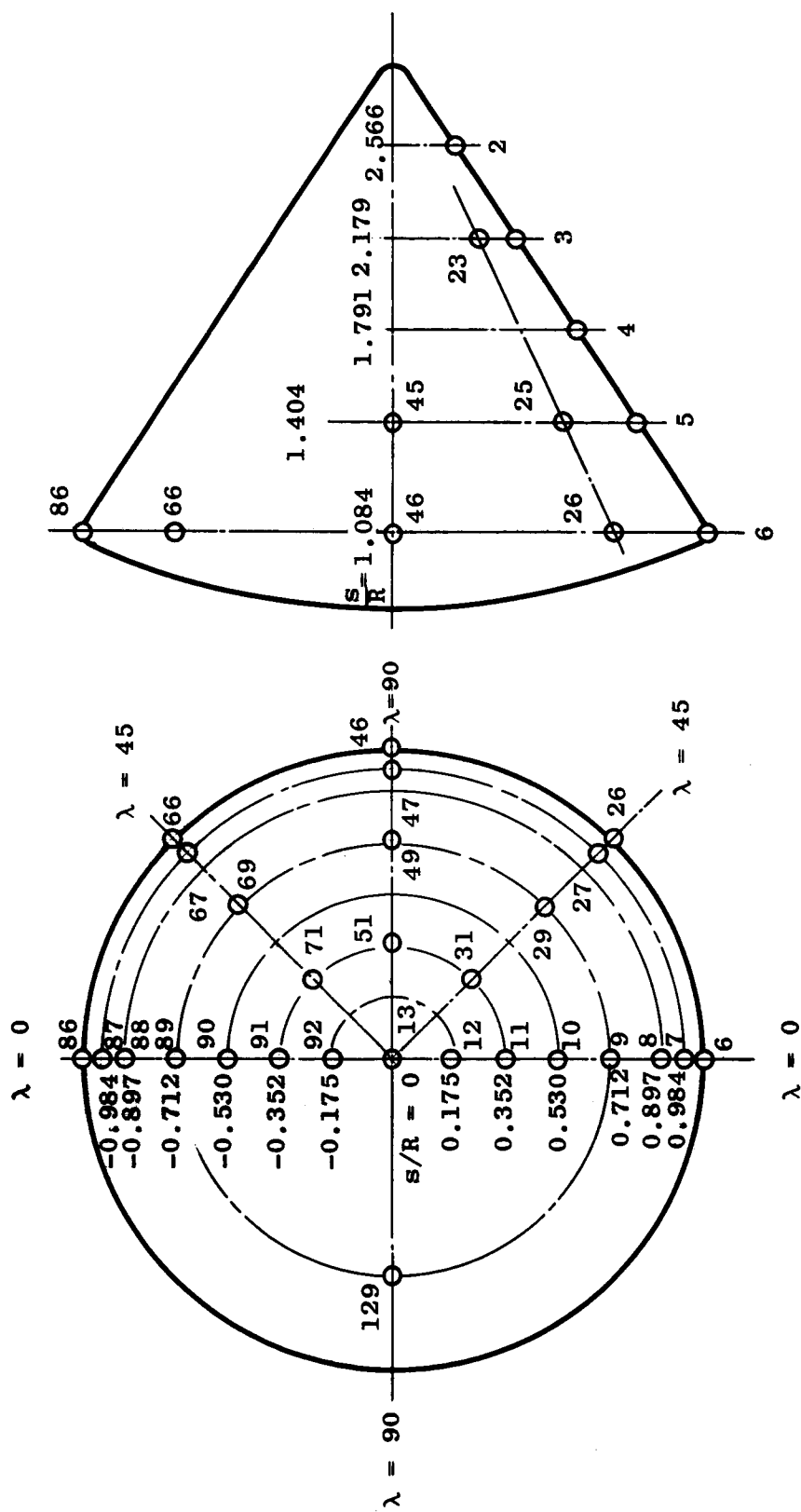


Fig. 4 Sketch of PS-4 Showing Pressure Orifice Locations

Solid Curve - Modified Newtonian Theory.

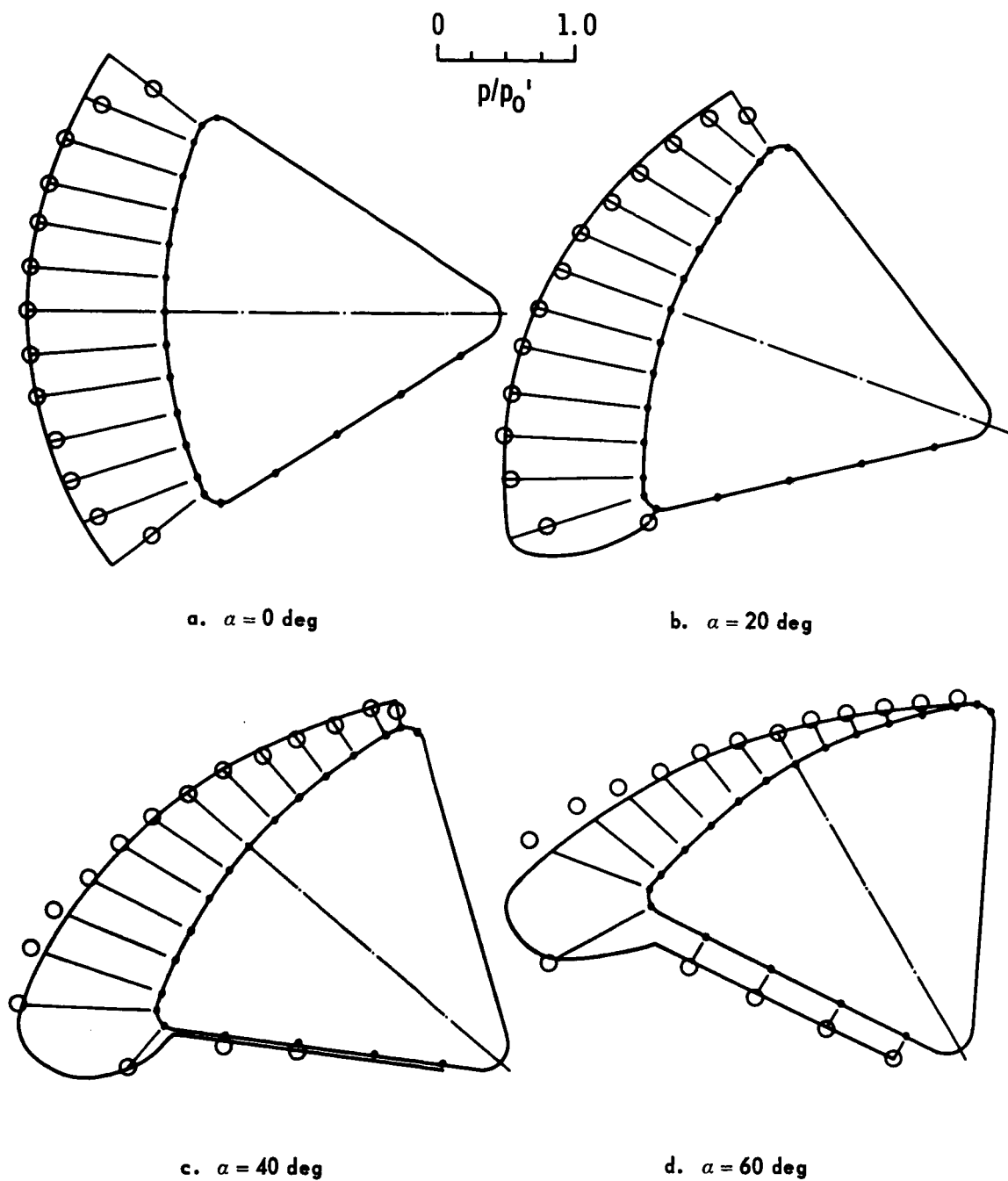


Fig. 5 Measured Pressure Distribution on PS-4

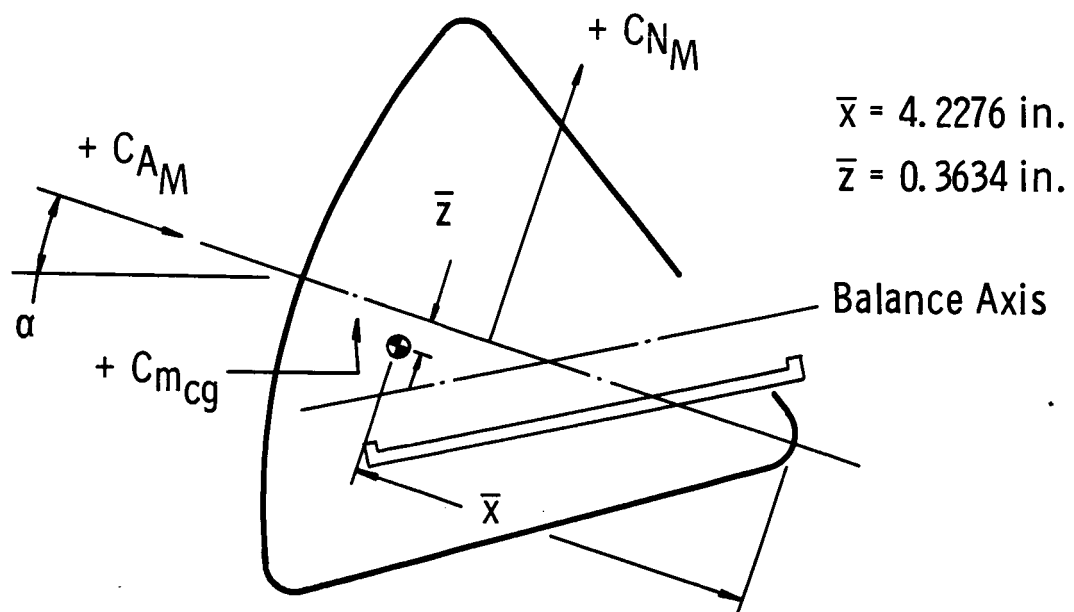
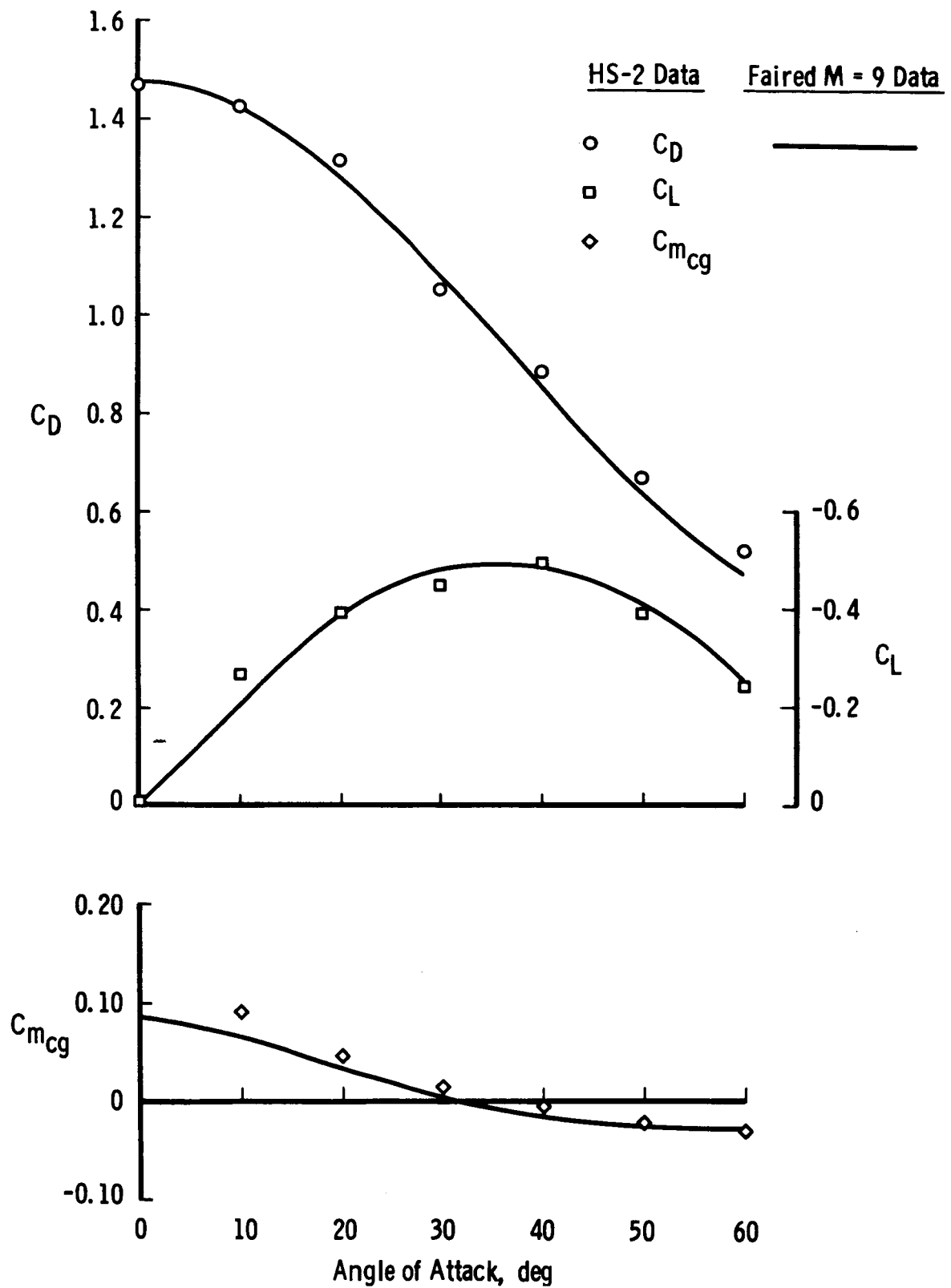


Fig. 6 Sketch of Model Showing Positive Directions of Model Coefficients

Fig. 7 Data Plots of C_L , C_D , and $C_{m_{cg}}$

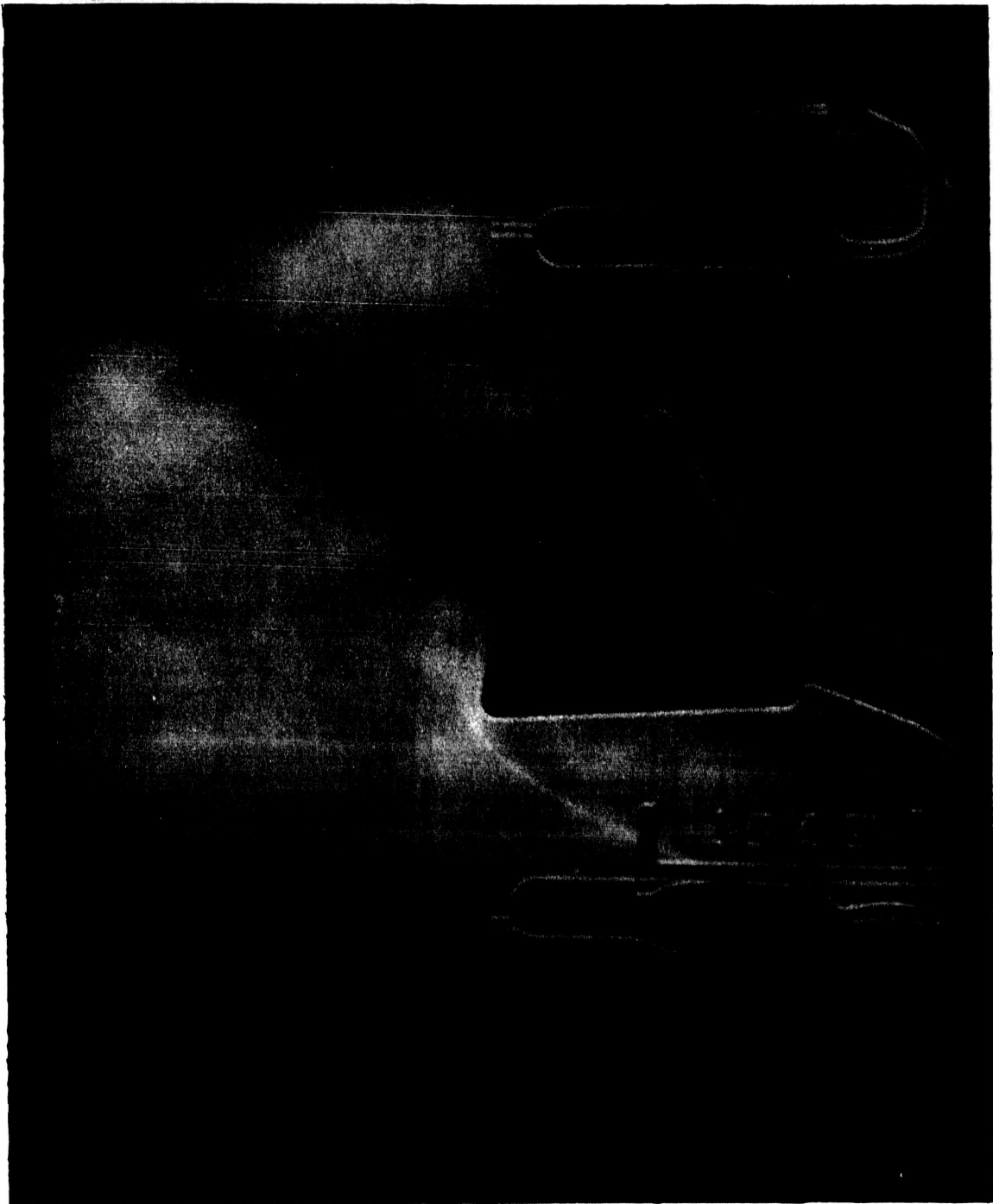


Fig. 8 Typical Schlieren Photograph of PS-4 Model